Available online at www.sciencedirect.com
ScienceDirect
Journal of Power Sources 172 (2007) 991–998
JOURNAL OF POWER SOURCES
www.elsevier.com/locate/jpowsour

Synthesis and electrochemical capacitance of binderless nanocomposite electrodes formed by dispersion of carbon nanotubes and carbon aerogels

Tarik Bordjiba, Mohamed Mohamedi *, Lê H. Dao

INRS-Énergie, Matériaux et Télécommunications, University of Quebec, 1650 Blvd. Lionel Boulet, Varennes, Quebec, Canada J3X 1S2

Received 6 April 2007; received in revised form 6 May 2007; accepted 8 May 2007
Available online 13 May 2007

Abstract

Novel nanocomposite carbon aerogel (CAG)-multi-walled carbon nanotubes (MWNT) materials have been synthesized and studied in 5 M KOH for electrochemical capacitor applications. The amount of MWNT in the nanocomposite was varied from 3 to 10 wt%. High specific surface areas ranging between 670 and 710 $m^2 g^{-1}$ were obtained as measured by nitrogen gas adsorption method, whereas the average pore diameter ranged between 1 and 4 nm.

Adding MWNT to the pristine CAG greatly improved the electrical conductivity as measured by electrochemical impedance spectroscopy. Finally, capacitance as high as 218 $F g^{-1}$ was obtained with a composite containing 3 wt% of MWNTs.

Keywords: Carbon paper substrate; Carbon nanotubes; Carbon aerogel; Nanocomposite binderless electrodes; Electrochemical capacitor technology

1. Introduction

Recent trends in electrochemical capacitor technology involve the development of high-surface area activated carbon electrodes to optimize the performance in terms of capacitance and overall conductivity [1,2]. Attention has been focused on nanostructured carbons, such as aerogels [3–11], nanotubes [12–17], nanotemplates [18] and carbon nanotubes-polymer composites [19–28]. Because of their unique architecture, high mechanical strength, tailorable electronic properties, extremely high surface areas, lightweight, and excellent chemical and thermal stability, carbon nanotubes are now intensively studied as new electrode materials for electrochemical capacitor structures. As to carbon aerogels, their advantages for capacitor application lie mainly in their high surface area, low ionic and electronic charging resistance and in their potential use as binderless electrodes. Furthermore, both the porosity and surface area of carbon aerogels can be controlled over a broad range, while the pore size and particle size can be tailored to the nanometer scale [29]. Replacing the standard carbon fiber with carbon aerogel electrodes could improve capacitance and cycleability.

However, the main weakness of the current carbon aerogel electrode lies on the expensive processing technology called supercritical drying, and the use of high cost precursor such as the resorcinol formaldehyde, from which the electrodes are made [29].

We have recently overcome these issues by developing a route to monolithic carbon aerogel electrodes that is made much easier and much less expensive to make than carbon aerogel electrodes, i.e., no supercritical drying step and no use of resorcinol formaldehyde were used in our process [5,6]. Moreover, our carbon aerogel are directly made on cheap support material such as carbon paper. The carbon paper is an electrically conductive material and acts thus as the current collector, which makes our materials very interesting as binderless electrodes for electrochemical power applications.

Aerogels are constituted of agglomerate particles linked by covalent bridges (ladder structure). The contact between these particles and the space due to the pores unfortunately introduce a high internal resistance within the aerogel. This lead to high equivalent series resistance ESR values which are detrimental to the power density for electrochemical capacitor technology. In order to reduce the internal resistance, strategies to introduce

* Corresponding author. Tel.: +1 450 929 8231; fax: +1 450 929 8102.
E-mail address: mohamedi@emt.inrs.ca (M. Mohamedi).

0378-7753/$ – see front matter.
doi:10.1016/j.jpowsour.2007.05.011

internal molecular nanocollectors (nanopathways for charges) such as carbon nanotubes imbibed in the porous matrice of the aerogel itself are being pursued in our laboratory and elsewhere.

It is important to stress that our purposes are not limited to taking well-known materials for electrochemical capacitor applications and combine them together. Because of their nanometer scale and high aspect ratio, fabrication and investigation of nanotubes/aerogel composites present considerable challenges. The effective utilization of carbon nanotubes in composite applications depends strongly on the ability to disperse the CNTs individually and uniformly throughout the CAG matrix without destroying their integrity or reducing their aspect ratio.

This work will present the synthesis of carbon aerogel-multi walled carbon nanotubes composite electrode material processed from their dispersion in dimethylformamide, and discuss their use as binderless electrodes in electrochemical capacitors. A variety of characterization techniques such scanning electron microscopy (SEM), microRaman, and specific surface area combined with electrochemical techniques were employed.

2. Experimental

2.1. Synthesis of carbon aerogel

Polyacrylonitrile (PAN) powder was purchased from Aldrich Chemical Co., and carbon paper (CP) sheets Technimat purchased from Lyndall Technical Papers. The preparation of PAN aerogels has been described previously [5,30]. Briefly, carbon paper sheets were dipped into a boiling solution of PAN (5 g) in a mixture of dimethylformamide (DMF)/water (84/16 mL). Afterwards, the sheets were dried in air for 10 min, and then immersed in acetone overnight. Thereafter, the sheets were dried in air before the pretreatment and carbonization processes. The pretreatment process was performed in air at 215 °C for 20 h. This important step led to cyclization reactions and to a ladder structure. Finally, the carbonization process was performed at 850 °C for 8 h in an inert atmosphere (argon), leading to the carbon aerogel denoted hereafter CAG.

2.2. Synthesis of carbon aerogel–carbon nanotubes composites

Purified multi-walled carbon nanotubes powder was purchased from Sigma–Aldrich and used as received (BET specific surface area as measured by us was of ca. 370 $m^2 g^{-1}$).

First, MWNTs were dispersed ultrasonically in DMF for 30 min. Then the resulting solution was added to PAN powder and the whole was further ultrasonicated for 30 min. Afterwards, the solution was stirred and heated until 140 °C, then appropriate amount of deionised water is added drop by drop. The two faces of carbon paper sheet were then dipped in the boiling solution and the resulting composite film (PAN-MWNT-CP) is dried in air for 10 min followed by soaking in acetone overnight. The exact amounts of the starting materials were of 0.15, 0.3, and 0.6 g MWNTs added to 5 g of polyacrylonitrile powder to prepare PAN-3 wt%MWNT, PAN-6 wt%MWNT and PAN-12 wt%MWNT, respectively.

Finally, the PAN-MWNT samples are dried in air before the pretreatment and carbonization processes similar to these applied to carbon aerogel (Section 2.1). At the end, three nanocomposites CAG-*x* wt%MWNT samples were prepared and denoted hereafter as CAG-3%MWNT, CAG-6%MWNT and CAG-12%MWNT.

2.3. Activation of CAG and CAG-MWNT composites

Carbonized CAG and CAG-MWNT samples were activated under carbon dioxide treatment. The activation was carried out using the following soak cycle: heating from ambient temperature to 800 °C during 1 h, holding at 800 °C under argon flow during 45 min. The atmosphere is then changed to mixture of argon/carbon dioxide during 15 min and then maintained to 800 °C during 1 h under carbon dioxide. Finally, the atmosphere is switched to argon gas and the temperature is cooled down to the ambient temperature.

2.4. Physical characterization

The specific surface area (SSA) was determined from nitrogen adsorption isotherms at 77 K (Autosorb-1 Quantachrome instrument) using the standard Brunauer, Emmett and Teller (BET) equation.

The morphologies of the samples were observed by scanning electron microscopy (SEM) using a JEOL, JSM 6300F apparatus. Micro-Raman measurements were taken with an RM 1000 Renishaw Raman Microscope System equipped with a laser at 514 nm, a Leica microscope and an electrically refrigerated CCD camera. The spectra shown here were obtained with 20 × magnification objective lenses. The laser output was 50 mW. Time acquisition was 5 min. The software employed for data acquisition and analysis was WIRE for Windows and Galactic Industries GRAMS/32TM. Ten scans were recorded to improve the signal-to-noise ratio. Spectra at three different points were taken for each sample to minimize problems arising because of the possible lack of sample uniformity. The Raman spectra presented are the representative measurements of the three points.

2.5. Electrochemical studies

Electrochemical measurements were carried out using a three-electrode cell with the reference electrode and counter electrode being an Ag/AgCl and a platinum coil, respectively. The mass loading (m) per unit of area of one electrode was 0.36, 0.47, 0.20, and 0.21 mg per 0.7 cm^2 electrode area for CAG, CAG-3%MWNT, CAG-6%MWNT, and CAG-12%MWNT, respectively. We have to emphasize that CAG-MWNT ratios represent the ones before activation. After activation, it is difficult or practically impossible to measure the CAG-MWNT ratio for this type of electrode structure. The electrolyte was 5 M KOH for all experiments. The sample electrochemical characteristics were determined by cyclic voltammetry (CV), constant current (CC) charge–discharge, and electrochemical impedance spectroscopy (E.I.S). An EG&G

galvanostat-potentiostat model 263A was used for CV, and CC measurements. The EIS measurements were conducted in the constant potential mode by sweeping the frequencies from 100 kHz to 0.01 Hz range at an ac-amplitude of 10 mV using Solartron 1255 frequency response analyser.

In our experiment samples were of 1 cm^2 area and only 0.7 cm^2 area was immersed in the electrolyte. The electrical connections to the potentiostat were made by crocodile clips to the non-immersed area. The crocodile clips were not thus in contact with the electrolytic solution. All the experiments were conducted at 25 °C.

2.6. Specific capacitance

The values of capacitance were estimated by voltammetry by integrating the total charge passed by the sample and dividing by the voltage window, i.e., $C = (1/2m) \times (1/\Delta E) \times \int I dt$, where I, t, ΔE, and m are the current (charge or discharge), time, CV voltage range and the mass of the electrode active material, respectively.

The capacitance from the constant current charge–discharge results was calculated using the equation $C = I \times t_d/m\Delta E_{CC}$, where I is the total current, t_d the discharge time, ΔE_{CC} is the CC potential drop during constant current discharge.

3. Results and discussion

3.1. Morphological and structural characteristics

The CAG-MWNT surface characteristics obtained by BET N_2 adsorption–desorption technique are listed in Table 1, along with these of the pristine CAG for reference. Within the CAG-MWNT composites, the following remarks can be made: (i) both the pore volume (PV) and the average pore diameter (PD) increased as function of the MWNTs content. A plot (not shown here) of PV and PD versus the MWNTs content resulted in a response that could be nicely fitted to a linear relationship with a regression factor of 0.997. This indicates that by varying the MWNTs content in the CAG-MWNTs composite, it is possible to tune the dimension of the pores for specific applications. (ii) As compared to pristine CAG, the SSA for the CAG-MWNT composites remained high and was almost unaffected by the MWNTs content (only a 5% decrease is seen).

Table 1
BET analysis (N_2 77 K adsorption) of the carbonized aerogel (CAG) and composite samples CAG-MWNTs

Sample	S_{BET} ($m^2\ g^{-1}$)	Pore volume ($cm^3\ g^{-1}$)	Pore diameter (nm)
CAG	772	0.367	1.91
CAG-3%MWNT	710	0.340	1.95
CAG-6%MWNT	676	0.443	2.62
CAG-12%MWNT	670	0.603	3.59

3.2. Microstructures of the CAG-MWNT composites

Typical SEM images of the bare carbon paper, CAG and CAG-MWNT nanocomposites are shown in Fig. 1. The CAG surface shows a highly porous structure easily accessible by the electrolyte (Fig. 1b). This material looks like a sponge with a highly connected structure. Fig. 2c–e shows SEM micrographs of the CAG-MWNT composites for various MWNT loadings. The morphologies of the CAG-MWNT nanocomposites are found to vary with the loaded wt% of MWNT. It can be seen that few MWNTs are located at the surface of the composite, where they connect the pores following highways architecture.

3.3. Micro-Raman analysis

Raman spectra for the pure MWNTs, the CAG and the CAG-MWNTs samples are shown in Fig. 2. The MWNT samples exhibited mainly two Raman bands at 1343 cm^{-1} (D band) and 1583 cm^{-1} (G band). The G band indicates original graphite features, whereas the D band is known to be related to disorder features of graphitic structures [31]. It is well known that the R-value, the relative intensity ratio of the D band to the G band depends on both the degree of graphitization and the alignment of the graphitic planes of carbon materials [32]. Also, the R-value is sensitive to the ratio of the concentration of graphite edge planes and/or crystal boundaries relative to standard graphite planes, i.e., the lower the R-value, the higher is the amount of sp^2 (graphite) clusters that exist on the sample. The intensity ratios of D band to G band (I_D/I_G) were determined and are reported in Fig. 3a, whereas the dependences of the Raman shift are illustrated in Fig. 3b.

The Raman spectra results, shown in Figs. 2 and 3, indicate that the specimens differ in graphitization degree. The deduced R-value for pure MWNTs sample is almost unity. On the other hand, the as-prepared CAG displayed the lowest R-value of ca. 0.58. Adding MWNTs to CAG increased the R-value, which further increased with increasing MWNT content in the CAG-based MWNTs, representing the transformation of graphitic carbon into disordered carbon.

The D and G band positions (Fig. 3b) for the CAG-MWNT sample decreased slightly as compared to the CAG-free MWNTs. However, it can be seen that the amount of MWNTs in the CAG-MWNTs composites had no significant effect on the D and G band positions.

3.4. Electrochemical characterization

Cyclic voltammograms carried out at 5 mV s^{-1} on CAG and CAG-MWNT composites in 5 M KOH are shown in Fig. 4. The current plots are normalized for the mass of active material in the electrode. The analysis of the curves shows a quasi-rectangular shape over an 800 mV range and there is no current peak caused by a redox reaction, indicating a typical electric double layer (EDL) behavior. From the dotted box drawn in Fig. 4, it is possible to identify the regions where deviations from ideal behavior are present. For the CAG sample, the deviation is higher and become less apparent with the addition of MWNTs. The main

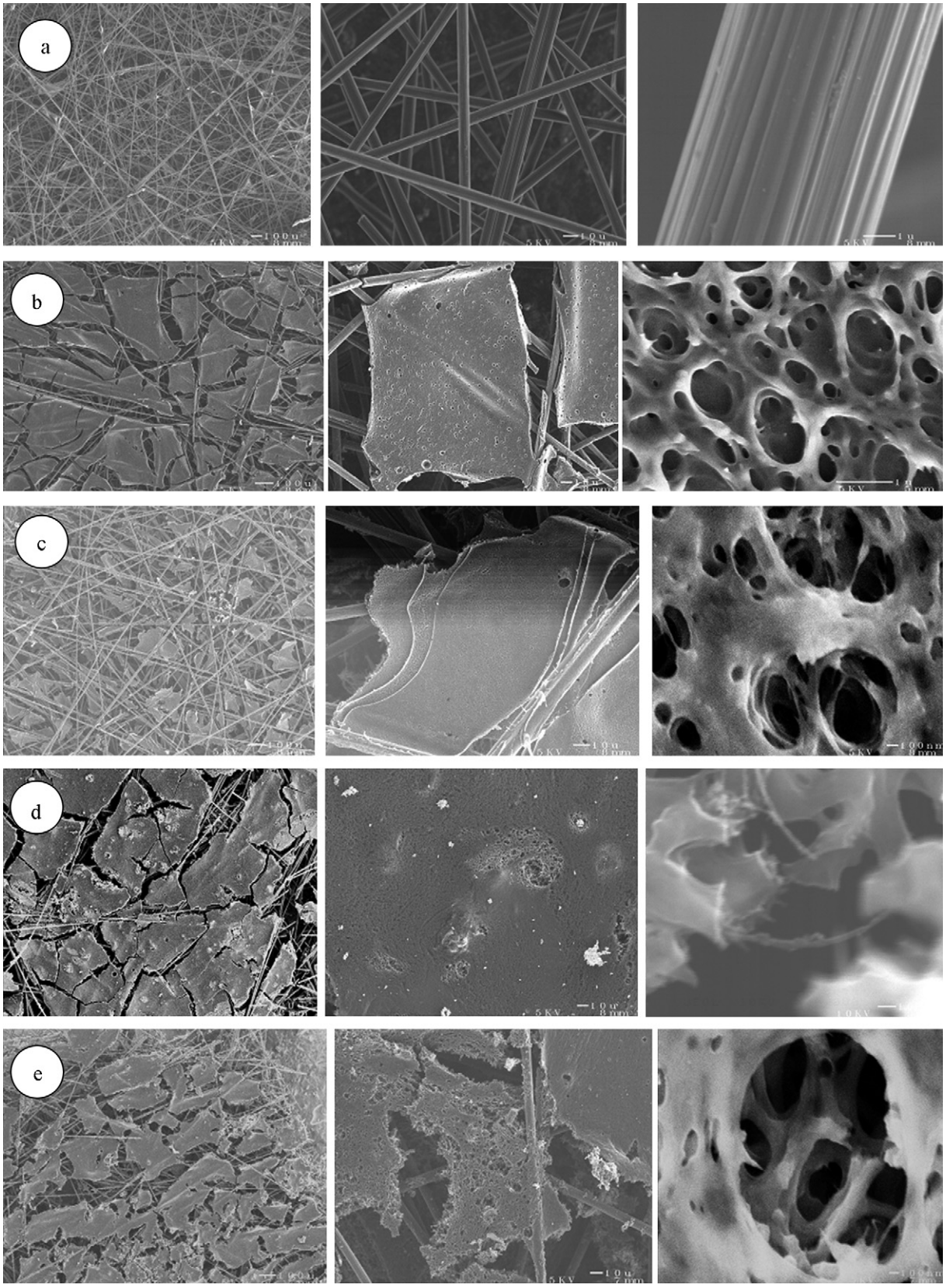

Fig. 1. SEM image of (a) bare carbon paper substrate, (b) CAG, (c) CAG-3%MWNT, (d) CAG-6%MWNT, and (e) CAG-12%MWNT. In each of the (a)–(e) are shown three images under increased magnification.

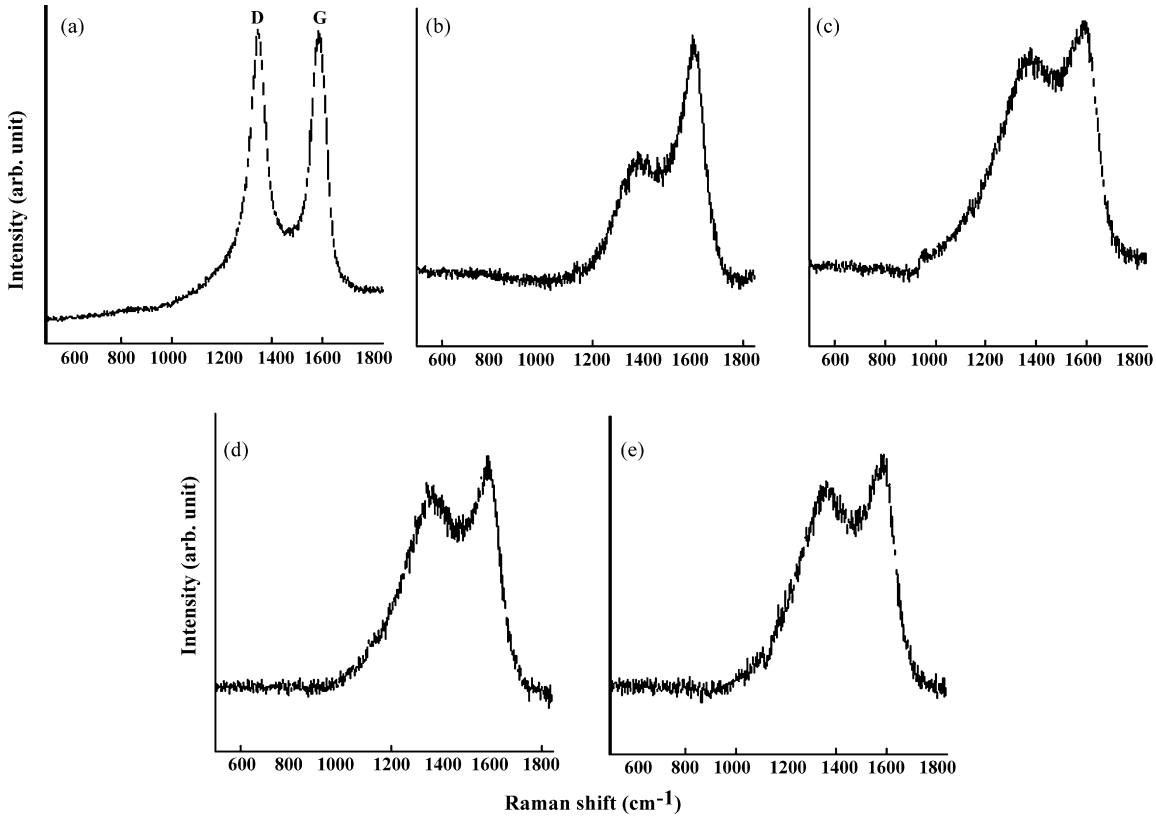

Fig. 2. Micro-Raman spectra (a) MWNTs, (b) CAG, (c) CAG-3%MWNT, (d) CAG-6%MWNT, and (e) CAG-12%MWNT.

causes of these deviations as explained in the introduction section are likely due to the inherent distributed resistance in the CAG porous electrodes, which appears after voltage inversion when the electric current should instantaneously change sign [33–35].

Results of experiments on the CAG and CAG-MWNT composite electrodes conducted at scan rates ranging from 5 to 100 mV s^{-1} showed that the current increases with increase of the scan rate for all the samples with no significant degeneration of the shape of the cyclic voltammograms at the high scan rates. Typical capacitances as function of electrode material and scan rate are reported in Fig. 5. It can be seen that capacitances obtained with CAG-3%MWNT are higher than those of CAG, i.e., 211 F g^{-1} versus 153 F g^{-1} at 5 mV s^{-1}. On the other hand, it seems that an amount of MWNTs higher than 3 wt% did not yield to any significant change in the capacitances as compared to pristine CAG.

Nevertheless, it is well-known that a correct estimation of specific capacitance should be done from constant current (CC) charge–discharge but not from voltammetry.

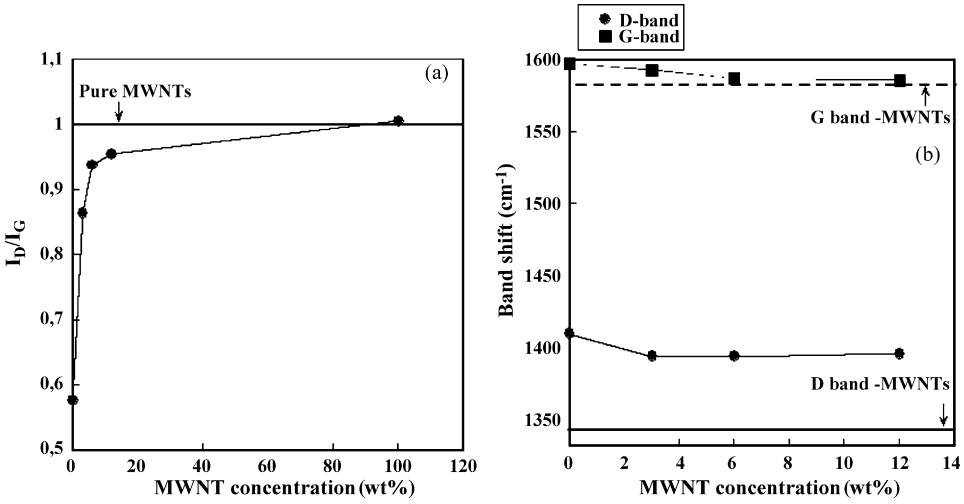

Fig. 3. Plots of (a) the relative intensity, $R = I_D/I_G$, and (b) peaks (G and D) position as function of MWNTs concentration.

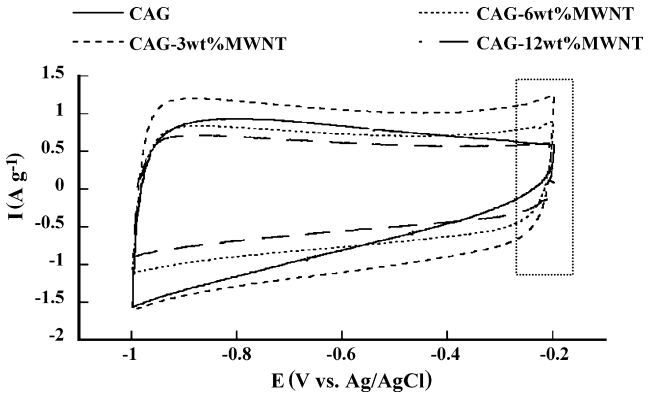

Fig. 4. Cyclic voltammograms of the CAG and CAG-MWNT samples, in 5 M KOH at room temperature, using a scan rate of 5 mV s^{-1}.

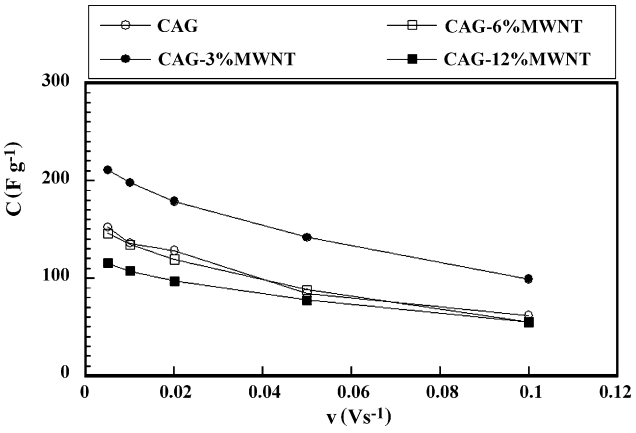

Fig. 5. Variation of the capacitance determined from cyclic voltammetry as function of the scan rate.

Typical CC charge–discharge cycles (cell voltage versus time) at a current of 1 mA are presented in Fig. 6. With the exception of CAG sample, the galvanostatic charge–discharge curves are close to linearity for all the CAG-MWNTs samples. CAG-MWNT composites demonstrated lower ESR than pure CAG, where the voltage drops at the very earlier period of charge–discharge switching is noticed. Capacitances determined as function of the applied current are reported in Fig. 7. It can be seen that capacitance of the CAG significantly decreased as the applied current increased, whereas that of the CAG-MWNT composites displayed good stability. This shows that MWNTs are very effective in decreasing the internal resistance of the CAG and by that demonstrating the effectiveness of the CAG-MWNTs synthesis procedure. An average capacitance of 134.4, 218, 156, and 122 F g^{-1} for the CAG, CAG-3%MWNT, CAG-6%MWNT, and CAG-12%MWNT, respectively. Unlike CV results (Fig. 5) that showed only the CAG-3%MWNT displaying capacitance higher than the pristine CAG, the CC results show that both CAG-3%MWNT and CAG-6%MWNT displayed higher capacitance that the pristine CAG with however the highest value still for the former sample.

Electrochemical impedance spectroscopy measurements (EIS) measurements at CAG and CAG-MWNT nanocompos-

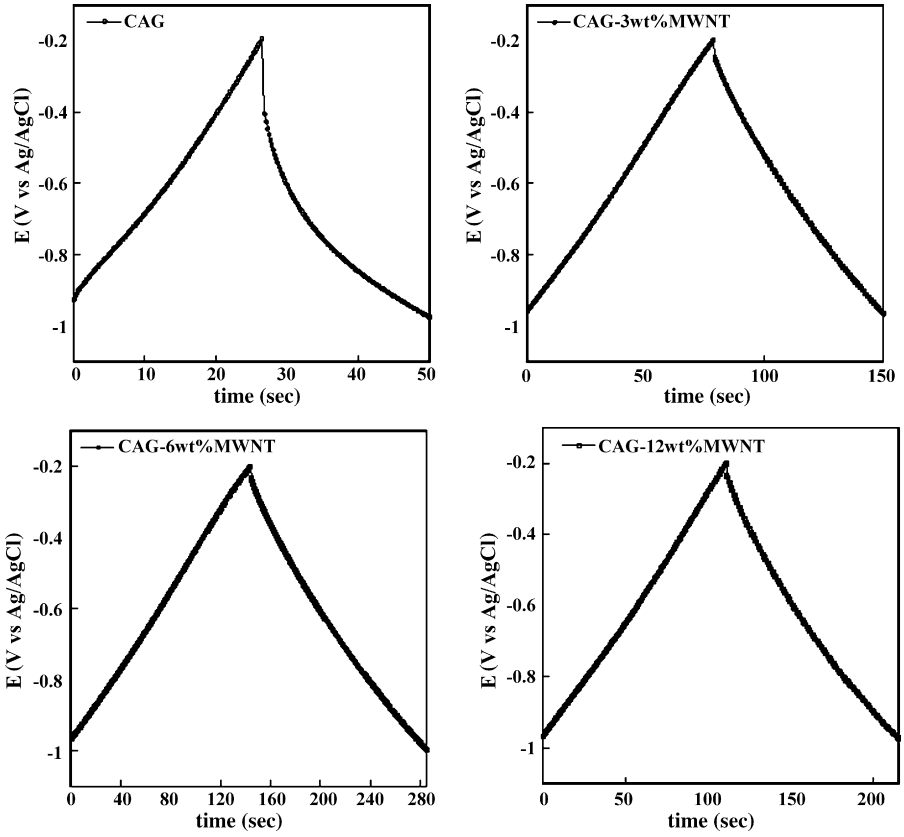

Fig. 6. Typical constant current charge/discharge curves at a current of at 1 mA for the CAG and CAG-MWNT nanocomposites.

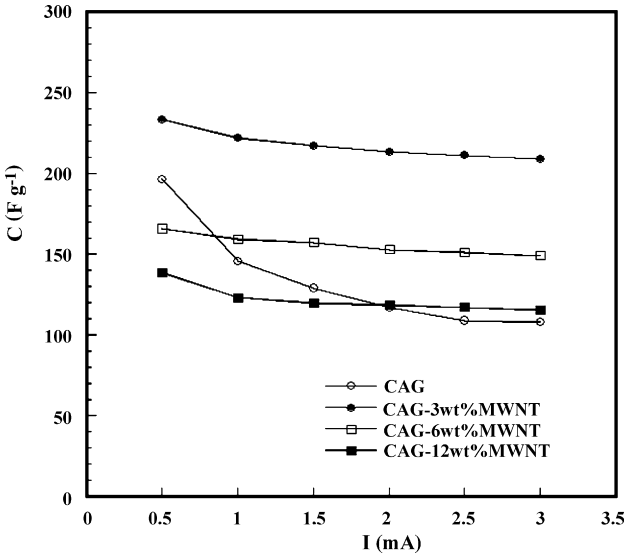

Fig. 7. Variation of the capacitance as function of the applied current for the CAG and CAG-MWNT nanocomposites.

ites were performed at −0.6 V versus Ag/AgCl and resulting spectra are displayed in form of Nyquist (Fig. 8a and b). If the time constants for the different processes are sufficiently different, the spectra in Fig. 8a and b comprise in general of (i) at the high-to-medium frequencies a semicircle of which diameter decreases as the MWNTs amount increases; (ii) In the low frequency range, a straight line with a slope of 45° from the real axis is observed that corresponds to semi-infinite Warburg impedance, which traduces ion penetration in the thickness of the porous structure of the electrode [36–38]; and (iii) with the exception of the CAG pristine, at the very low frequencies a more or less vertical line, which is due to the accumulation of ions at the bottom of the pores of the electrode at the measurement's potential is observed for the CAG-MWNT nanocomposites. The vertical dependence of the imaginary part demonstrates a good capacitive behavior without diffusion limitations.

Since no faradic current was observed in cyclic voltammetry (Fig. 4), the semi-circle cannot be ascribed to a charge-transfer process. The semi-circle rather reflects the sum of the electrolyte resistance and to the contact resistance between the nanocomposites (the electrode itself) and the carbon paper (current collector). Indeed as observed in Fig. 8, the diameter of the semi-circle depends on the MWNT content in the CAG-MWNT nanocomposite, i.e., the diameter of the semi-circle decreased as the MWNT content increased, which simply means that with the nanotubes added, better contact is being made to the coated carbon paper.

Electrode conductivity improvements, if they were happening, should show up as a decrease in the ESR (intersection point of the impedance with the real axis in the very low frequency region). In fact the complex-plane impedance for the CAG-MWNT nanocomposites containing 3–12 wt% of the MWNT do show that ESR (the drawn inclined line in Fig. 8b) decreased as the MWNTs content increased. This decrease in the internal resistance in the CAG-MWNT nanocomposite is further demon-

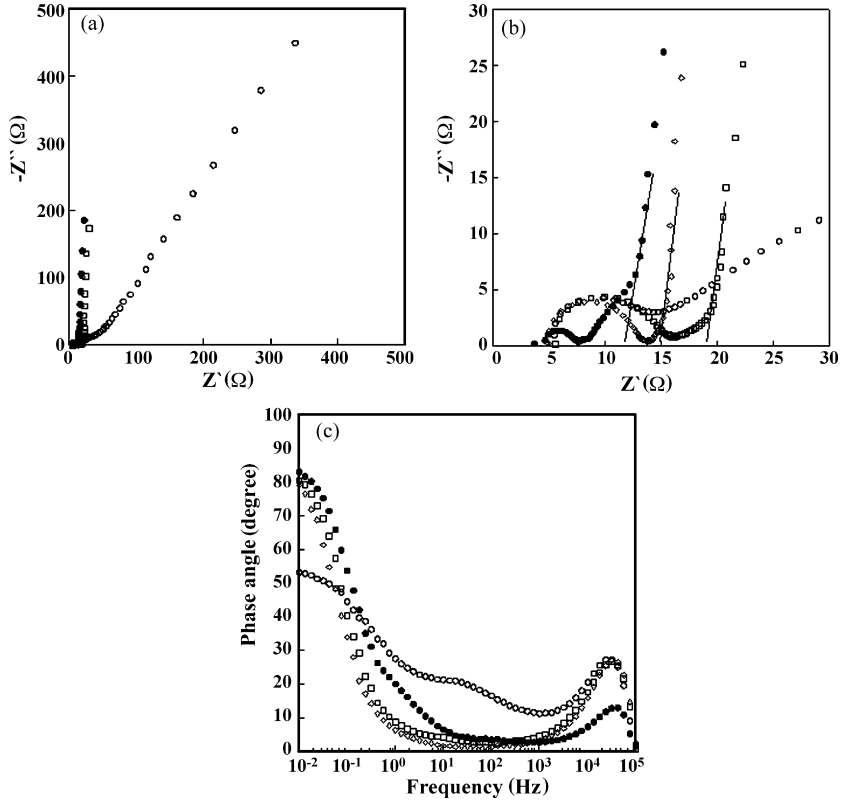

Fig. 8. Impedance spectra of a three-electrode cell containing 5 M KOH aqueous electrolyte, with different working electrodes: (◯) CAG, (□) CAG-3%MWNT, (◊) CAG-6%MWNT, and (●) CAG-12%MWNT. (a) Nyquist plot, (b) magnification of the high frequency region of (a), and (c) Bode plot.

strated by the Bode plot of Fig. 8c, where one can see that with increasing amounts of MWNT, the phase angle at the low frequency region is close to 90°. These observations indicate that MWNT are acting as efficient nanopathways for charges in the in the porous matrice of the carbon aerogel.

4. Conclusions

New cost-effectively nanocomposite materials based on carbonized polyacrylonitrile-multi walled carbon nanotubes materials processed from their dispersion in dimethylformamide have been synthesized and studied for electrochemical capacitor applications. The composites displayed high specific surface area ranging between 670 and 710 $m^2\,g^{-1}$.

Addition of MWNTs up to 6 wt% to CAG improved both the specific capacitance and the conductivity of the CAG. A maximum capacitance as high as 218 $F\,g^{-1}$ was however obtained with a nanocomposite containing 3 wt% of MWNTs.

Stability of CAG and CAG-MWNTs nanocomposites upon several thousands of galvanostatic charge–discharge cycling in conjunction with elemental composition (X-ray photoelectron spectroscopy), and structural studies (microRaman spectroscopy) carried out before and after cycling are in progress.

Acknowledgments

This work was supported by Natural Sciences Engineering Research Council of Canada (NSERC Discovery grant), CSA (Canadian Space Agency, Materials Program), The Canadian Foundation for Innovation (FCI), and INRS-EMT.

References

[1] A. Burke, J. Power Sources 91 (2000) 37.
[2] A.S. Aricò, P. Bruce, B. Scrosati, J.-M. Tarascon, W. Van Schalkwijk, Nat. Mater. 5 (2005) 366.
[3] R.W. Pekala, J.C. Farmer, C.T. Alviso, T.D. Tran, S.T. Mayer, J.M. Miller, B. Dunn, J. Non-Cryst. Solids 225 (1998) 74.
[4] J. Wang, S.Q. Zhang, Y.Z. Guo, J. Shen, S.M. Attia, B. Zhou, G.Z. Zheng, Y.S. Gui, J. Electrochem. Soc. 148 (2001) D75.
[5] P. Gouérec, H. Talbi, D. Miousse, F. Tran-Van, L.H. Dao, K.H. Lee, J. Electrochem. Soc. 148 (2001) A94.
[6] H. Talbi, P.-E. Just, L.H. Dao, J. Appl. Electrochem. 33 (2003) 465.
[7] W. Li, H. Pröbstle, J. Fricke, J. Non-Cryst. Solids 325 (2003) 1.
[8] J.W. Long, B.M. Dening, T.M. McEvoy, D.R. Rolison, J. Non-Cryst. Solids 350 (2004) 97.
[9] S.-W. Hwang, S.-H. Hyun, J. Non-Cryst. Solids 347 (2004) 238.
[10] H.-J. Kim, J.-H. Kim, W.-I. Kim, D.J. Suh, Korean J. Chem. Eng. 22 (2005) 740.
[11] Y.-Z. Wei, B. Fang, S. Iwasa, M. Kumagai, J. Power Sources 141 (2005) 386.
[12] B. Zhang, J. Liang, C.L. Xu, B.Q. Wei, D.B. Ruan, D.H. Wu, Mater. Lett. 51 (2001) 539.
[13] K.H. An, W.S. Kim, Y.S. Park, Y.C. Choi, S.M. Lee, D.C. Chung, D.J. Bae, S.C. Lim, Y.H. Lee, Adv. Mater. 13 (2001) 497.
[14] E. Frackowiak, K. Jurewicz, S. Delpeux, F. Béguin, J. Power Sources 97–98 (2001) 822.
[15] Ch. Emmenegger, Ph. Mauron, P. Sudan, P. Wenger, V. Hermann, R. Gallay, A. Züttel, J. Power Sources 124 (2003) 321.
[16] F. Picó, J.M. Rojo, M.L. Sanjuán, A. Ansón, A.M. Benito, M.A. Callejas, W.K. Maser, M.T. Martínez, J. Electrochem. Soc. 151 (2004) A831.
[17] J.-S. Ye, X. Liu, H.F. Cui, W.-D. Zhang, F.-S. Sheu, T.M. Lim, Electrochem. Commun. 7 (2005) 249.
[18] P.A. Nelson, J.R. Owen, J. Electrochem. Soc. 150 (2003) A1313.
[19] K. Jurewicz, S. Delpeux, V. Bertagna, F. Béguin, E. Frackowiak, Chem. Phys. Lett. 347 (2001) 36.
[20] K.H. An, K.K. Jeon, J.K. Heo, S.C. Lim, D.J. Bae, Y.H. Lee, J. Electrochem. Soc. 149 (2002) A1058.
[21] R. Saito, R. Matsuo, T. Kimura, G. Dresselhaus, M.S. Dresselhaus, Chem. Phys. Lett. 348 (2001) 187.
[22] T.V. Sreekumar, T. Liu, B.G. Min, H. Guo, S. Kumar, R.H. Hauge, R.E. Smalley, Adv. Mater. 16 (2004) 58.
[23] G.Z. Chen, M.S.P. Shaffer, D. Coleby, G. Dixon, W. Zhou, D.J. Fray, A.H. Windle, Adv. Mater. 12 (2000) 522.
[24] M. Wu, G.A. Snook, V. Gupta, M. Shaffer, D.J. Fray, G.Z. Chen, J. Mater. Chem. 15 (2005) 2297.
[25] Y.-K. Zhou, B.-L. He, W.-J. Zhou, H.-L. Li, J. Electrochem. Soc. 151 (2004) A1052.
[26] M. Hughes, M.S.P. Shaffer, A.C. Renouf, C. Singh, G.Z. Chen, D.J. Fray, A.H. Windle, Adv. Mater. 14 (2002) 382.
[27] V. Khomenko, E. Frackowiak, F. Béguin, Electrochim. Acta 50 (2005) 2499.
[28] F. Béguin, K. Szostak, G. Lota, E. Frackowiak, Adv. Mater. 17 (2005) 2380.
[29] J.D. Lemay, R.W. Hopper, L.W. Hrubesh, R.W. Pekala, MRS Bull. 15 (1990) 19.
[30] P. Gouérec, D. Miousse, F. Tran-Van, L.H. Dao, J. N. Mater. Electrochem. Syst. 2 (1999) 221.
[31] M.S. Dresselhaus, G. Dresselhaus, R. Saito, A. Jorio, Phys. Rep. 409 (2005) 47.
[32] F. Tuinstra, J.L. Koenig, J. Chem. Phys. 53 (1970) 1126.
[33] K. Kinoshita, Carbon Electrochemical and Physicochemical Properties, Wiley, New York, USA, 1988.
[34] F. Lufrano, P. Staiti, M. Minutoli, J. Electrochem. Soc. 151 (2004) A64.
[35] K.H. An, K.K. Jeon, W.S. Kim, Y.S. Park, S.C. Lim, D.J. Bae, Y.H. Lee, J. Korean Phys. Soc. 39 (2001) S511.
[36] R. de Levie, Electrochim. Acta 8 (1963) 751.
[37] H. Keiser, K.D. Beccu, M.A. Gutjahr, Electrochim. Acta 21 (1976) 539.
[38] D.D. Macdonald, M. Urquidi-Macdonald, S.D. Bhakta, B.G. Pound, J. Electrochem. Soc. 138 (1991) 1359.